Journal of Applied Fluid Mechanics, Vol. 17, No. 7, pp. 1354-1367, 2024.
Available online at www.jafmonline.net, ISSN 1735-3572, EISSN 1735-3645.
https://doi.org/10.47176/jafm.17.7.2342

Comparative Analysis of Turbulence Models for Evaluating the Aerodynamic Characteristics of Bus

T. Huang[1], J. Ma[1], D. Yi[1], X. Ren[1], R. Ke[1], C. Ou[1†], Q. Du[1], Q. Huang[1] and W. Zeng[2]

[1]*College of Mechanical Engineering, Hunan Institute of Science and Technology, Yueyang, PR China*
[2]*Department of Mechanical Engineering, New York Institute of Technology, New York, USA*

†Corresponding Author Email: 12012014@hnist.edu.cn

ABSTRACT

In order to determine the most suitable turbulence model for studying the aerodynamic performance of bus, the effects of different turbulence models on the aerodynamic characteristics of bus were investigated. A comparative analysis was conducted on five turbulence models (IDDES, DDES, DES, LES, URANS). The pressure distribution on the cross section at x=0 and y=0 is also analyzed for each model. The results reveal that IDDES accurately captures the negative pressure at the rear of the bus and predicts the pressure gradients more effectively than other models. IDDES also captures more vortices at the head of the bus and predicts the wake flow more widely than other models. DDES has obvious shedding phenomenon in the wake flow, while IDDES provides a relatively smooth airflow trajectory, but its prediction of airflow trajectory at a distance is less clear. Through quantitative and qualitative analyses of the aerodynamic characteristics of bus under different turbulence models, it can be concluded that IDDES is the most suitable turbulence model to study the aerodynamic characteristics of bus.

Article History

Received September 30, 2023
Revised January 10, 2024
Accepted February 3, 2024
Available online April 30, 2024

Keywords:

Aerodynamics characteristic
Flow field
Turbulence
Vortex
Wake

1. INTRODUCTION

As highways continue to rapidly develop, bus are becoming more prevalent. Unlike sedans, bus have large bodies that lack a streamlined structure (Altaf et al., 2014; Kongwat et al., 2020). As a result, they produce a strong wake at high speeds, leading to significant aerodynamic drag and lift (Volpe et al., 2015; Garcia-Ribeiro et al., 2023). This can significantly impact the bus's driving stability and fuel economy (Mohamed et al., 2015; Li et al., 2016).

Several researchers have conducted wind tunnel tests and road experiments to investigate the aerodynamic characteristics of bus. For instance, François et al. (2009) examined the aerodynamic properties of a double-decker bus through wind tunnel experiments, where they measured the pressure distribution on the front and side of the bus, as well as the drag and lateral force. Dorigatti et al. (2012) obtained the lateral force, lift force, and rolling moment of vans, bus, and trucks by conducting wind tunnel tests. These vehicles were placed on bridge models with a 1:40 scale. However, these experimental methods have limitations in terms of capturing detailed pressure distribution and flow around the bus body due to the experimental conditions and environment, as well as the high cost and time-consuming nature of the experiments. These limitations significantly hinder the development of bus aerodynamics. Conversely, Computational Fluid Dynamics (CFD) can overcome these difficulties as it offers high-speed, cost-effective, and safe operation capabilities.

Up to date, there have been a number of scholarly studies (Ashagrie et al., 2017; Jadhav & Chorage, 2020) that have contributed to the understanding of the aerodynamic performance of bus. The findings provide valuable insights for improving driving stability, reducing aerodynamic drag, and enhancing the efficiency of commercial bus through aerodynamic optimization. Numerous studies have utilized CFD to investigate the aerodynamic characteristics of bus, where the utilization of a reasonable turbulence model is essential. For instance, Krajnovic & Davidson (2003) employed the Large eddy simulation (LES) model to analyze the flow around a simplified bus and found that instantaneous flow differs significantly from the time-averaged flow not only in the wake but also along the entire body. Kanekar et al. (2017) used the standard k-ε model to investigate the aerodynamics of a Maharashtra state transport bus and discovered that modifying the design decreased the drag coefficient by 28% and improved fuel

NOMENCLATURE

C_d	drag force coefficient	S	Vorticity tensor
C_l	lift force coefficient	W	width of bus model
H	height of bus model	W_T	width of computational domain
H_T	height of computational domain	Ω	rate tensor
L	length of bus model	ρ	air density
L_T	length of computational domain	τ_{jx}	residual stresses
Q	Q Criterion		

economy by 20% at a speed of 80 km/h. Winkler et al. (2016) employed detached eddy simulation (DES) model to capture vehicle performance to evaluate aerodynamics and vehicle dynamics. Zhao et al. (2019) investigated the influences of crosswind angle and longitudinal spacing on bus platoon by standard k-ε model. It is revealed that the drag coefficient of the bus increases first and then decreases with the increase of crosswind angle. Yudianto et al. (2021, 2022) investigated the alteration of the aerodynamic coefficients of a bus under various conditions using the SST k-ω turbulence model. Alonso-Estébanez et al. (2017) studied the impact of bridge deck configuration on the aerodynamic coefficients of a bus under crosswind using RANS. Chang et al. (2021) based on LES and DES, reliable numerical calculation method of flow and aero-noise on coach was established and verified. Although these studies have contributed significantly to the field, the most suitable turbulence model for studying the aerodynamic characteristics of the bus remains unclear. Therefore, it is necessary to investigate the aerodynamic characteristics of the bus under different turbulence effects and identify the best turbulence model.

Numerous scholars have compared various turbulence models for vehicles such as trains, trucks, and blunt bodies. For instance, He et al. (2022) assessed LES, Improve Delay Detached Eddy Simulation (IDDES), and Unsteady Reynolds Averaged Naviver Stokes (URANS) models for predicting the flow around streamlined high-speed trains. The LES model was found to be suitable for studying the aerodynamic characteristics of such trains. Wang et al. (2017) used URANS, Scale Adaptive Simulation (SAS), and DES models to predict the flow field of a general train model, and all three models were able to predict the time-averaged and transient flow characteristics, as well as longitudinal vortex and spanwise oscillation. Similarly, He et al.(2021) and Serrea et al. (2013) evaluated different turbulence models for predicting the flow field around the Ahmed body, with the LES and IDDES models found to produce consistent results with experimental data. Patel et al. (2019) compared the aerodynamic coefficient and surface pressure of trucks under LES and RANS models, with the LES model providing more detailed information about the complex flow structure around trucks. Additionally, Cheng et al. (2011) simulated the flow around road vehicles using LES and RANS models, showing that unsteady aerodynamics can be utilized for stability control. Numerous scholars also used a specific turbulence model to discuss aerodynamic problems (Gu et al., 2016; Huang et al., 2017; Gilotte et al., 2022; Probst & Melber-Wilkending 2022; Zheng et al., 2022). In addition, several studies (Bhattacharya & Ahmed, 2010; Joshi & Bhattacharya, 2019; Anzalotta et al., 2020; Joshi et al., 2023) have provided valuable insights for further research and the development of innovative aerodynamic methods. These studies collectively explore different aspects of aerodynamics, including fluid dynamics simulations, and wake dynamics. It also provide a foundation for understanding fluid dynamic phenomena, as well as for engineering applications to improve aerodynamic performance. Comparative research on the aerodynamic performance of bus by using different turbulence models is still lacking. Thus, this study will conduct in-depth research in this field.

In this study, five different turbulence models were employed to study the aerodynamic performance of bus. Section 2 provides a detailed description of the bus model, simulation method and wind tunnel experiments. Then the aerodynamic characteristics of the bus under different turbulence models were analyzed qualitatively and quantitatively.

2. COMPUTATIONAL MODEL

2.1. Bus Model and Computation Domain

To optimize computational resources and time, a simplified version of the bus model was used without sacrificing accuracy by excluding elements such as the rear-view mirrors and wiper. The full-size simplified model of the bus is depicted in Fig. 1(a), with dimensions of 3.565 m in height (H), 2.500 m in width(W), and 11.942 m in length(L).

To ensure that the flow field is fully developed, a rectangular computational domain is used in this study, as shown in Fig. 1(b). The dimensions of the computational domain are set to a length (L_T) of 135.11 m, a height (H_T) of 17.83 m, and a width (W_T) of 44.90 m. The inlet boundary is set to a velocity boundary with

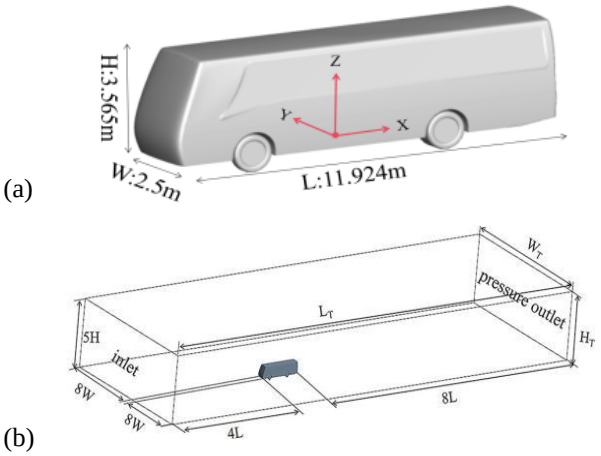

Fig. 1 Illustration of the bus model: (a) simplified geometry of the bus model; (b) computational domain

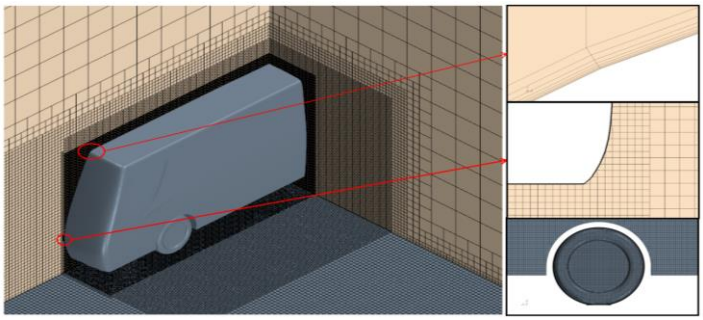

Fig. 2 Grid

a velocity of 30 m/s, which is consistent with the wind tunnel test. The Reynolds number, based on the characteristic length of the vehicle body, is 2.385×10^7. And the characteristic length of the vehicle body which was used to calculate Reynolds number is 11.924 m. The outlet boundary is set to a pressure outlet boundary. The ground, top, left and right sides of the wind tunnel are set as no-slip walls. The front end of the bus is located 4L from the inlet boundary, while the rear end is located 8L from the outlet boundary. The height of the computational domain is set to 5H, and the distance between the bus and the left and right walls is 8W, respectively.

2.2. Grid Generation and Grid Independence Verification

To ensure accurate flow field data and optimize computational resources, this study utilizes two types of grids in the computational domain. The dense areas around the body surface are covered with triangular prism grids, while the rest of the domain employs hexahedral grids. The size of fine meshes around the bus is 50 mm and the size of coarse meshes is 100 mm. To ensure the continuity, consistency, and isotropy of field quantities across different scales of grid, linear interpolation method is employed to generate new data points on the fine grid by interpolating between existing data points on the coarse grid. The vehicle surface generates eight boundary layers, and a local grid refinement scheme is used to increase grid density around the bus and in the wake, while ensuring a smooth transition to a lower resolution away from the bus. The grid consists of three refinement areas: one for the body and two for the background. Figure 2 illustrates the grid, which was generated using commercial software STAR-CCM+.

In this study, three grid schemes are generated by adjusting the grid size near the vehicle to achieve different resolutions. Table 1 provide details of the grid resolutions used, with the height of the first layer of the grid on the entire model surface set to 0.05 mm to ensure the wall-normal resolution is less than 1. The rear of the vehicle has denser grids, providing higher resolution of the wake, while finer surface grids are used around the edges of the body. The streamwise and spanwise resolutions are both around 3. Table 2 shows the errors in C_d and C_l of IDDES model. To verify the grid independence, three different grid cases are used, as shown in Fig. 3. Based on a balance between computational accuracy and cost, the medium case is employed in this study.

Table 1 Details of the grids

case	coarse	medium	fine
Grid number	2.480×10^7	3.470×10^7	4.860×10^7
Wall-normal resolution	$n^+<1$	$n^+<1$	$n^+<1$
Streamwise resolution	$3<\Delta_s^+<40$	$3<\Delta_s^+<30$	$3<\Delta_s^+<20$
Spanwise resolution	$3<\Delta_l^+<28$	$3<\Delta_l^+<25$	$3<\Delta_l^+<20$

Table 2 Prediction of C_d and C_l in different grid case

Case	Coarse	Medium	Fine	EXP
C_d	0.4236	0.4402	0.4418	0.4525
Error	6.39%	2.72%	2.36%	
C_l	-0.1035	-0.1002	-0.0999	-0.0971
Error	6.59%	3.19%	2.88%	

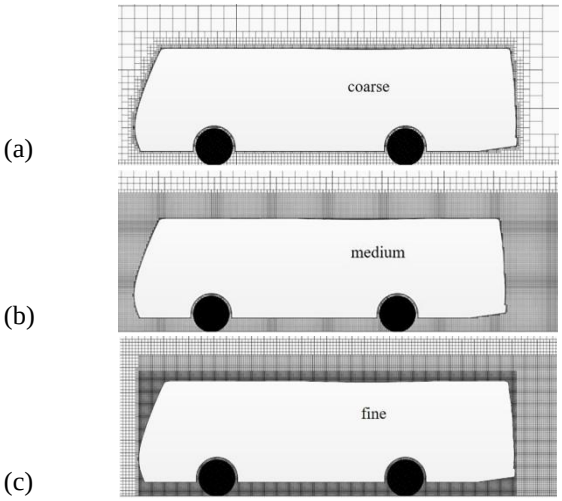

Fig. 3 Details of grids with different densities. (a) coarse; (b) medium; (c) fine

2.3. Experiment

To ensure the accuracy of the model, a wind tunnel test was conducted at the HD-2 wind tunnel of Hunan University. The length of test section is 17 m, with a rectangular cross-section measuring 2.5 m in height and 3 m in width. The maximum wind speed is 58 m/s and the contraction ratio is 3:2. The turbulence intensity is 0.13%. The aerodynamic force are measured by the six component balance. The wind speed in the wind tunnel is measured using a hot wire anemometer. The wind tunnel test setup is illustrated in Fig. 4.

Fig. 4 Wind tunnel test

2.4. Turbulence Model

Different turbulence models have their own capabilities in specific areas. For example, RANS is widely used in industrial flows, such as pipe flows and pollution dispersion prediction. LES is typically used for simulating complex turbulent flows, such as turbulent wakes, turbulent combustion, and turbulent eddies. DES is suitable for problems that require simulating both turbulent details and large-scale flow structures, such as aerodynamic noise prediction and hydrodynamic studies. (Argyropoulos & Markatos 2015; Spalart, 2015; Duraisamy et al., 2019; Salari & Ortega 2021). An incompressible gas assumption was employed in this study.

The basic equation is as follow,

$$\frac{\partial u_j}{\partial x_i} = 0 \tag{1}$$

$$\frac{\partial \overline{u}_i}{\partial t} + u_j \frac{\partial u_i}{\partial x_j} = f_i - \frac{1}{\rho}\frac{\partial p}{\partial x_i} + \frac{1}{\rho}\frac{\partial \tau_{jx}}{\partial x_j} \tag{2}$$

$$\rho c_p\left(\frac{\partial T}{\partial t} + u_j \frac{\partial T}{\partial x_j}\right) = \frac{\partial}{\partial x_j}(-q_j) + S \tag{3}$$

In this paper, several turbulence models such as URANS, DES, Delay Detached Eddy Simulation (DDES), IDDES and LES are used.

2.4.1. URANS

In the Reynolds-averaged Navier-Stokes (RANS) approach, the flow characteristics are decomposed into their mean and fluctuating components and time averaging is performed. On the other hand, in unsteady RANS (URANS), an additional unsteady term is included in the momentum equation. The URANS simulations in this study use the two-equation SST *k-ω* model (Menter, 1994). The SST *k-ω* model is capable of accurately predicting turbulent shear stress transfer, as well as handling inverse pressure gradient and zero pressure gradient (Nived et al., 2022). The standard form of SST *k-ω* model is as follows:

$$\frac{\partial(\rho k)}{\partial t} + \frac{\partial(\rho u_j k)}{\partial x_j} = P - \rho^* \rho \omega k + \frac{\partial}{\partial x_j}\left[(\mu + \sigma_k \mu_t)\frac{\partial k}{\partial x_j}\right] \tag{4}$$

$$\frac{\partial(\rho \omega)}{\partial t} + \frac{\partial(\rho u_j \omega)}{\partial x_j} = \frac{\gamma \rho}{\mu_t} P - \beta \rho \omega^2 + \frac{\partial}{\partial x_j}\left[(\mu + \sigma_\omega \mu_t)\frac{\partial \omega}{\partial x_j}\right] + 2(1-F_1)\frac{\rho \sigma_{\omega 2}}{\omega}\frac{\partial k}{\partial x_j}\frac{\partial \omega}{\partial x_j} \tag{5}$$

2.4.2. DES

In DES, a combination of RANS and LES models is used to solve the flow field. RANS is applied near the solid boundaries and in regions where the turbulence scale is smaller than the maximum grid size. When the turbulent length scale exceeds the grid size, LES is used to solve the flow field in the large eddy region, where large-scale unsteady turbulence dominates. In this region, DES restores the LES with a sub-grid model. In the near-wall area, RANS is restored (Spalart, 2009). This approach significantly reduces the computational cost of applying LES to high Reynolds number engineering problems. However, the accuracy and effectiveness of DES depend on the ability of the turbulence model to accurately switch between RANS and LES (Shur, et al. 2015). The equation for DES can be expressed as follows:

$$\frac{\partial \tilde{\nu}}{\partial t} + \bar{u}_j \frac{\partial}{\partial x_j}(\tilde{\nu}) = c_{b1}\tilde{S}\tilde{\nu} - c_{w1} f_w \left(\frac{\tilde{\nu}}{\tilde{d}}\right)^2 + \frac{1}{\sigma_{\tilde{\nu}}}\left\{\nabla \cdot \left[(\nu + \tilde{\nu})\nabla \tilde{\nu}\right] + c_{b2}(\nabla \tilde{\nu})^2\right\} \tag{6}$$

2.4.3. DDES

Although the DES model can produce better results than the RANS model in many cases, it has been found that when calculating the flow separation of certain smooth surfaces, the position of the separation is sensitive to the total Reynolds stress. Moreover, when DES switches from RANS to LES, the transition of the boundary layer may not be smooth (Deck & Renard, 2020; Mockett et al., 2015; Renard & Deck, 2015), resulting in the inability to switch to LES in some regions due to insufficient grid density. Consequently, the total Reynolds stress is low, and the separation occurs earlier. In such situations, the performance of DES is not between RANS and LES, but rather worse than RANS, which is unexpected. To address these issues, Spalart proposed further modifications, and Shur et al. (2008) introduced the DDES turbulence model, which redefines the length scale to resolve the problem of simulated stress degradation.

$$l_{DDES} = d - f_d - \max(0 - C_{DES}\Delta) \tag{7}$$

Where f_d is the delay function to realize the delay from RANS mode to LES mode.

2.4.4. IDDES

The RANS model can be used as the wall model directly, which is far away from the wall and coincides with LES. However, in fully developed channel flow experiments, it was found that the Log-Layer was divided into two segments that could not be matched, which is known as the Log-Layer Mismatch (LLM) (Reddy et al., 2014). The transition between RANS and LES causes the modeled Reynolds stresses to not transition smoothly and slowly, resulting in relatively low total Reynolds stresses. Consequently, the slope of the Log-Layer becomes problematic. To address this issue, Shur et al. (2008) introduced a new sub-grid length scale definition that depends on the wall distance, resulting in the IDDES model. The IDDES model not only successfully resolves the LLM problem but also performs better than the DDES model in some complex flow problems that involve walls.

The definition of grid filter in the IDDES model depends on the grid size and wall distance, as shown in the following formula:

$$\Delta = \min[\max(C_w d_w; C_w h_{\max}; h_{wn}); h_{\max}] \tag{8}$$

Where C_w= 0.15 is an empirical constant, h_{max} is the maximum of grid spacing in all three directions, and h_{wn} is the grid spacing in the normal direction of the wall. The length scale combination of LES and URANS is

$$l_{IDDES} = \tilde{f}_d(1+f_e)l_{URANS} + (1-\tilde{f}_d)l_{LES} \tag{9}$$

$$l_{URANS} = \sqrt{k}/0.09\omega \tag{10}$$

$$l_{LES} = C_{DES}\Delta \tag{11}$$

The function f_d is a mixed function between URANS and LES modes. In order to counteract the reduced turbulence in the boundary layer, the enhancement function f_e is regarded as a part of the definition of length scale.

2.4.5. LES

LES is a computational method used for calculating turbulence (Tyliszczak et al., 2014; Chaouat, 2017). It is based on the concept that the larger eddy structures are greatly influenced by the flow field, while the smaller eddies can be considered as isotropic. Thus, LES separates the simulation of large eddies from that of small eddies and calculates them using different models. In LES, the large eddy structures are filtered out from the flow field, leaving only the large eddies to be calculated. The small eddies are then solved by additional equations. The filtering scale is typically chosen as the grid scale.

In LES method, Φ is the filtered variable, which represents the spatially averaged quantity of the field at a particular location, rather than the time-averaged quantity (Friess et al., 2015). It can be obtained using the following formula:

$$\bar{\phi} = \int_D \phi G(x, x')dx \tag{12}$$

Where D is the flow area. X is the spatial coordinate. $G(x, x')$ is the filter function, which determines the scale of the solved vortex.

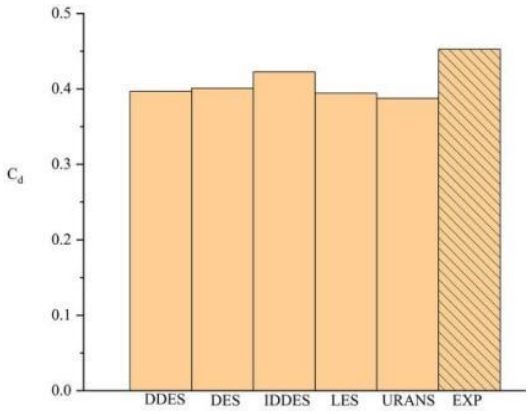

(a)

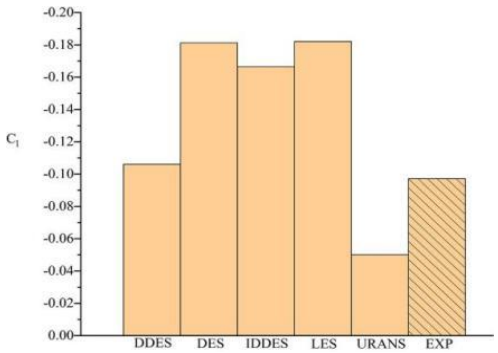

(b)

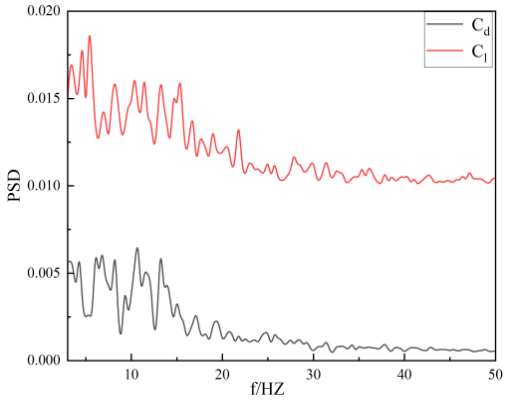

(c)

Fig. 5 (a) C_d; (b) C_l; (c) Power spectrum density

3. Result And Analysis

3.1. Coefficient of Aerodynamic Load

Figure 5 displays the drag coefficient (C_d) and lift coefficient (C_l) obtained from five different turbulence models. The experimental drag coefficient is 0.4525, which is closely approximated by all five turbulence models. The drag coefficient obtained from the URANS model is 0.3877, slightly lower than the other models, resulting in a difference of 0.0648 from the experimental result. In contrast, the drag coefficient obtained from the IDDES model is 0.4226, slightly higher than the other models, with a difference of only 0.0299 from the experimental result. The lift coefficient obtained from the experiment is -0.0971, as shown in Fig 5(b). It can be observed that there are some difference between the lift

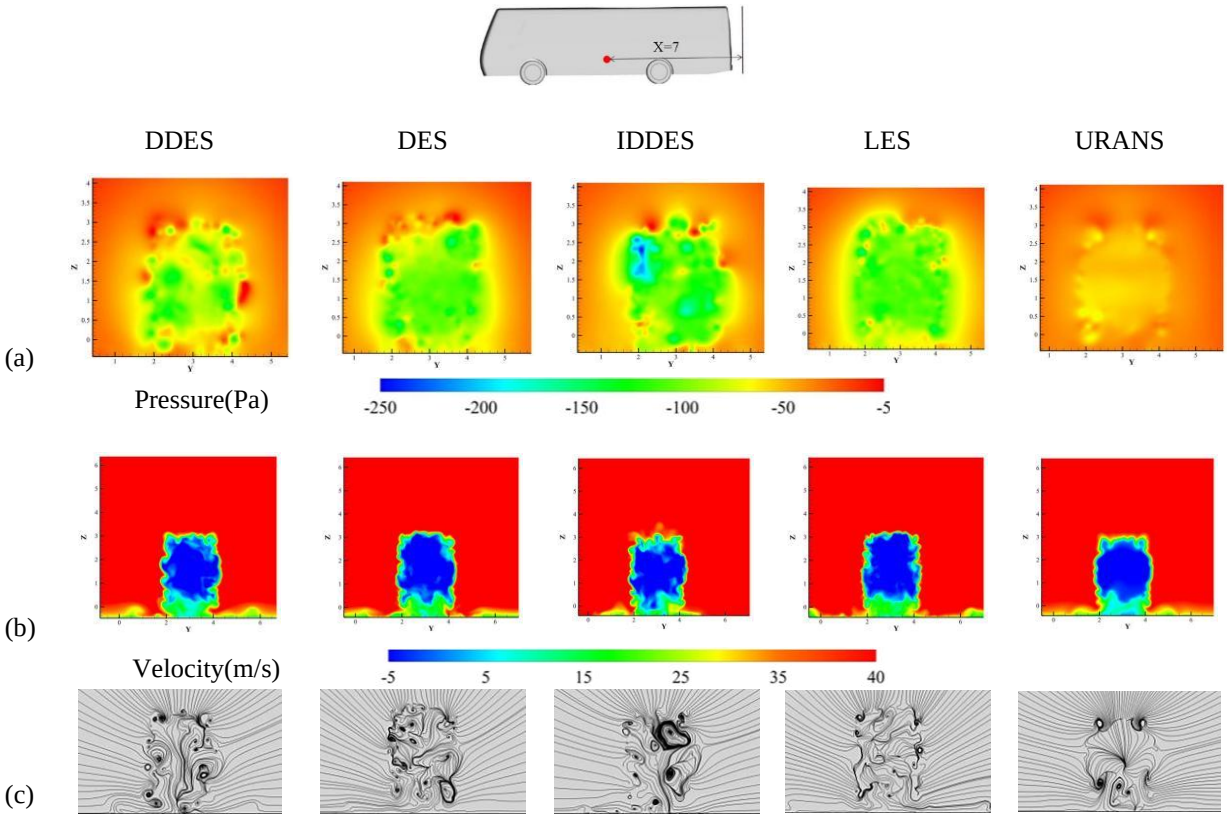

Fig. 6 Pressure, velocity and streamline distributions on x =7: (a) pressure; (b) velocity; (c) streamline

coefficient obtained from different models and the lift coefficient measured in the experiments. This difference is primarily due to geometric variations between the models used in simulations and the laboratory setups. The measurement process of the lift coefficient in experiments may be affected by measurement errors, such as sensor accuracy, calibration inaccuracies and so on. The lift coefficient obtained from the URANS model is -0.0500, significantly different from the experimental result. The flow around a bus exhibits complex unsteady turbulence structures, such as vortex shedding and vortex interactions. URANS model have limitations in capturing these details. The lift coefficients obtained from the DES, LES, and IDDES models are all significantly larger than the experimental result. However, the lift coefficient obtained from the DDES model is -0.1061, the closest approximation to the experimental result, with only a small difference of 0.0090. Thus, in terms of aerodynamic load coefficients, the DDES and IDDES models are more suitable for studying aerodynamic coefficients by addressing the problems of grid-induced separation and inconsistency of log-layer curves, respectively. Figure 5(c) shows the PSD of the lift coefficient exhibits high peak values and a more complex trend, it indicates that the bus is influenced by more nonlinear flow phenomena such as turbulence and wake interaction. This could be attributed to the non-uniformity of the flow.

3.2. Wake Flow

At high speeds, the airflow around the vehicle body produces separation, resulting in the formation of vortices and vortex shedding at the rear end. These phenomena significantly increase the vehicle's drag. The aerodynamic drag of the bus is also affected by the pressure distribution at the front and rear ends. The pressure change at the rear end of the bus body is particularly significant, so the pressure distribution at the rear greatly affects the aerodynamic drag of the bus (Zhang et al., 2020; Huang et al., 2023). Consequently, this section focuses on the distribution of wake flow.

Figure 6(a) displays the pressure distribution on a section located at the rear of the bus at x = 7. The turbulence models exhibit significant variations in the pressure distribution. The URANS model is not suitable for capturing the tail pressure due to its limitations in capturing negative pressure. This is mainly because the URANS model calculates the time-averaged flow field and filters out many small vortices through time-averaging. The DDES model exhibits more intricate pressure fluctuations and is more effective in capturing the pressure gradients at the rear, aligning closely with the actual driving conditions of a bus. Figure 6(b) shows the velocity distribution at the rear of the bus. The URANS model captures a symmetric velocity field distribution with inaccurate wake vortex and airflow trajectory compared to other turbulence models. This implies that the URANS model is not suitable for predicting the velocity distribution of the rear and wake vortex. The IDDES model captures more complex turbulence details at the top of the bus tail, indicating its capability of capturing the flow field changes at the rear end of the bus. Figure 6(c) displays the velocity streamline at the rear of the bus. The airflow trajectories of DDES and DES models are complex, whereas that of the IDDES model is relatively smooth, predicting the trends of flow well.

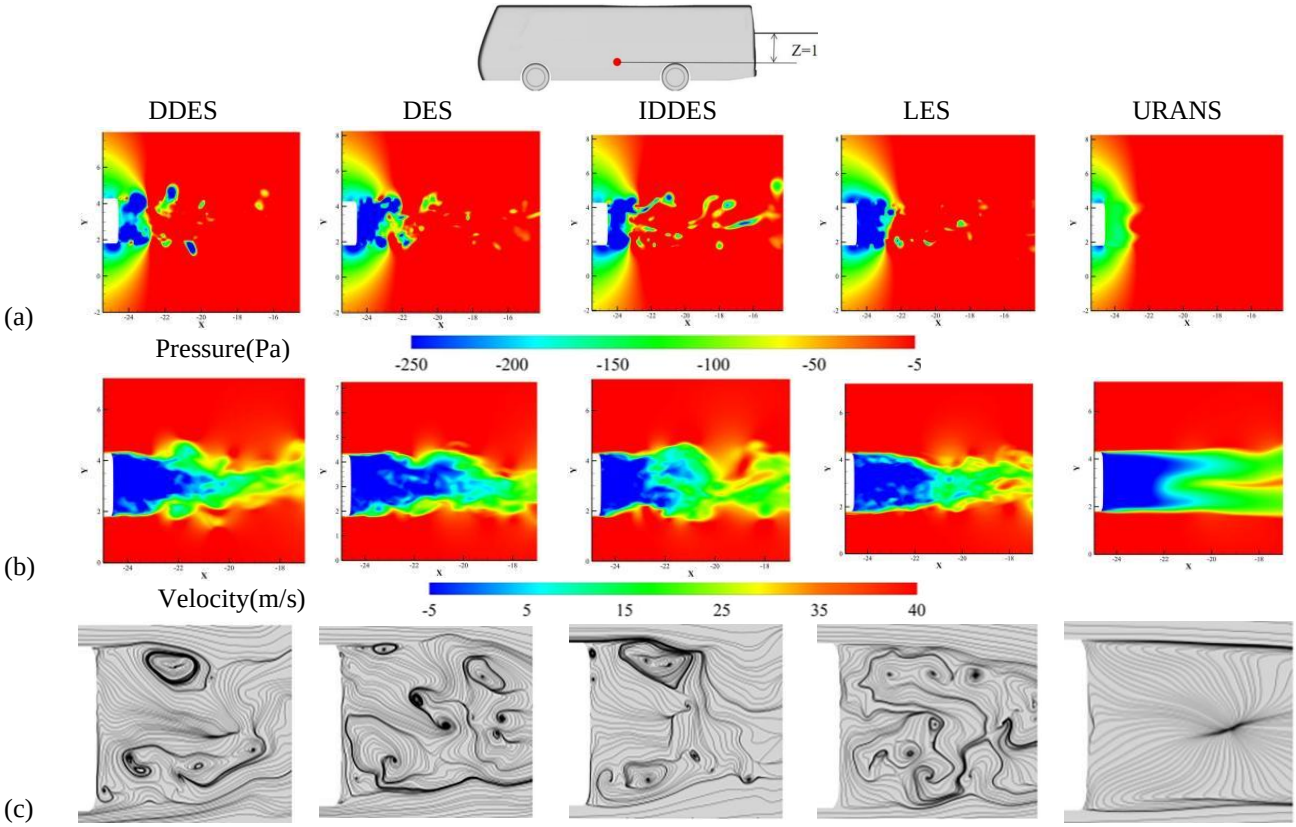

Fig. 7 Pressure, velocity and streamline distributions on z =1: (a) pressure; (b) velocity; (c) streamline

In Fig. 7, the pressure, velocity, and velocity streamline distributions on a cross-section located at z=1 at the rear end of the vehicle are presented. The spanwise pressure distribution captured by all five turbulence models is very similar. However, IDDES is able to predict further negative pressure in the flow direction pressure distribution, making it superior to the other three turbulence models. The IDDES turbulence model predicts more negative pressure values mainly due to its enhanced detached eddy simulation and improved turbulence closing model. DDES and DES models are better than LES model in capturing the pressure at a distance. URANS model's ability to capture pressure in the flow direction is not as good as the other turbulence models. In Fig. 7(b), the velocity distribution shows that IDDES model has a broader and larger area for predicting wake flow, but the speed fluctuation is obvious and not as even as LES model. The wake of DDES model falls off more quickly, and DES model doesn't show a good velocity gradient. Figure 7(c) shows velocity streamline, and the details of air flow trajectory captured by LES model are still the clearest, thanks to the filtering process of LES model. DDES, DES, and IDDES models have their own characteristics in capturing the air flow trajectory. The streamline in IDDES and DDES models are relatively smooth, while DES model captures more flow details. Both DDES and IDDES models are based on DES model, which is the product of adding RANS model equation and LES model equation together. It is equivalent to using RANS model in the boundary layer and using LES model outside the boundary layer. URANS model only captures the airflow on both sides of the bus, and most of the flow details are filtered out. Therefore, URANS model is also suitable for predicting the air flow trajectory.

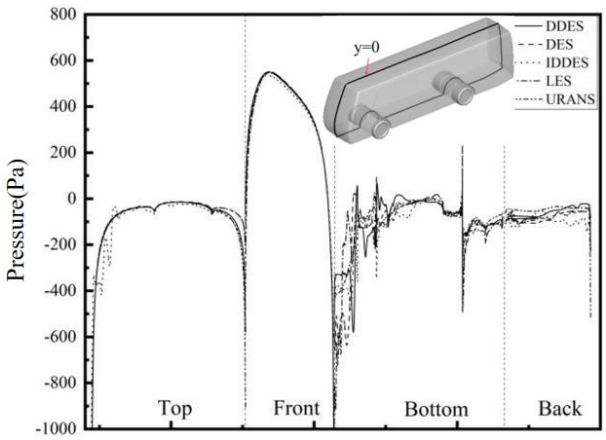

Fig. 8 Pressure distribution on y=0

Figure 8 shows the pressure distribution of bus along the y=0 line, as predicted by the DES, DDES, LES, URANS, and IDDES models. The models are generally in agreement, except for the IDDES model which shows a stepwise increase in pressure. The pressure gradients at the turning points of the front and bottom, front and top, and rear and bottom are evident in all models, except for the front and top and bottom and back turning points. The LES model captures the largest pressure gradient at the front and bottom turning point compared to the other models. The IDDES model predicts a slightly higher average pressure difference than the URANS, LES, IDDES, and DES models, which is consistent with the

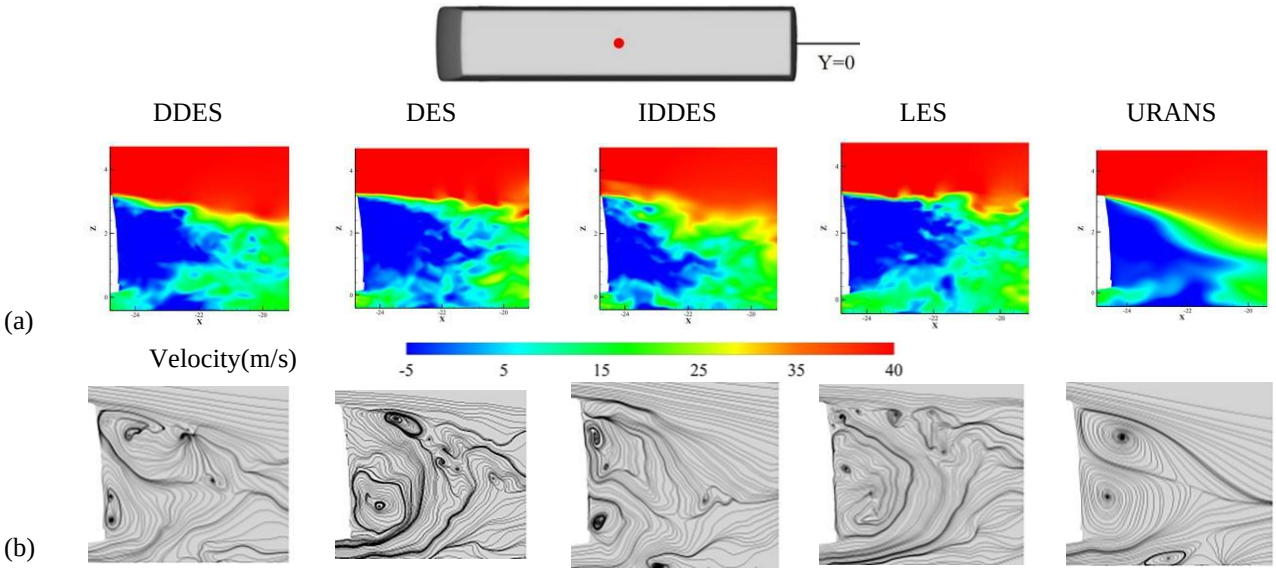

Fig. 9 Velocity and streamline distributions on y=0: (a) velocity; (b) streamline

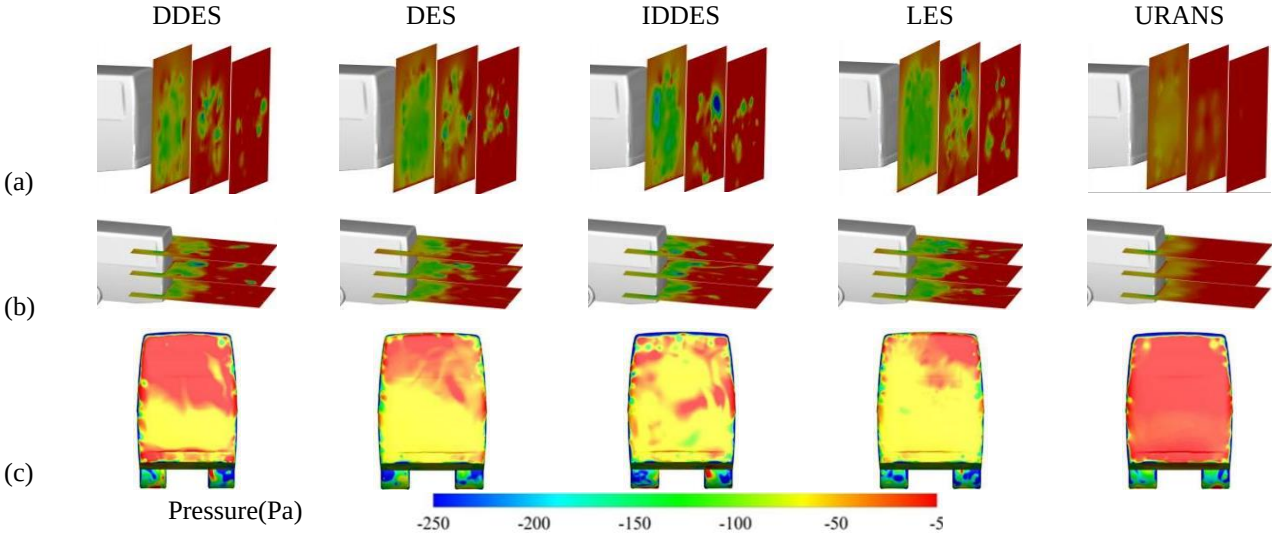

Fig. 10 (a) different x-plane pressure diagram at the rear; (b) different z-plane pressure diagram at the rear; (c) pressure diagram at the rear body surface

results obtained in section 3.1 regarding the drag coefficient.

As illustrated in Fig. 9(a), the LES model is able to generate the most uniform wake flow in the flow direction, while the wake flow predicted by IDDES model is closer to the ground and lacks clarity in the flow direction. The flow trajectories predicted by DES and IDDES models are more intricate than those predicted by the other three turbulence models, as depicted in Fig. 9(b). This better reflects the actual situation of air flow at the rear of the bus. However, the IDDES model fails to predict the long-distance flow trajectory. All the turbulence models, except for URANS, are able to form relatively complete wake vortices near the rear.

The turbulence separation at the rear of the bus is a complex phenomenon and a major contributor to the increase in driving drag. To better understand the pressure distribution at the rear of the bus, Fig. 10 presents an analysis of the pressure in this region.

Figure 10(a) presents the pressure distribution on the three surfaces at the rear end of the bus located at x=6, x=5, and x=4. The ability of different turbulence models to capture pressure at a distance is observed on the x=4 plane. The results show that LES model outperforms the other four turbulence models in capturing the pressure at the rear of the bus. The pressure predicted by LES model becomes more widely distributed towards x=4. In contrast, IDDES, LES, and DES models demonstrate better performance than DDES model in capturing the pressure in the distance. URANS model is relatively weak in capturing pressure on the x=4 cross section. Moreover, IDDES model is capable of capturing the significant high negative pressure on the x=5 section, which is superior to DES, LES, and DDES models. On the x=6 section, the pressure predicted by

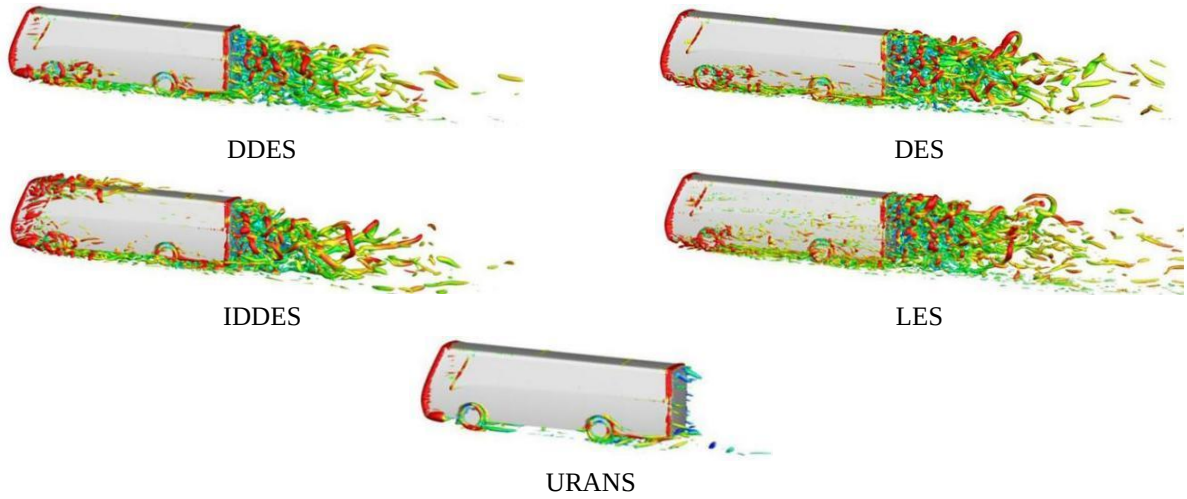

Fig. 11 Vortex with Q=1000

IDDES, LES, and DES models covers the entire plane, while URANS and DDES models fail to cover the plane.

The pressure distribution on three sections at z=0, z=1, and z=2 is depicted in Fig. 10(b). These results further confirm the findings that IDDES model performs better in capturing distance pressure and DDES model excels in capturing large vortex shedding on the z=1 section. Moreover, it is re-validated that the LES model provides a more uniform pressure distribution on all three planes compared to the other four turbulence models. LES captures turbulent details more accurately by resolving and simulating the smaller-scale turbulent structures within the wake. This enables LES to provide more realistic and refined turbulence simulation results. Specifically, it is less dispersed than the DES model and not as minimal as the URANS model.

In Fig. 10(c), the pressure distribution at the rear of the bus body is depicted, and it is evident that different turbulence models yield different pressure distributions. The IDDES model captures a more complex pressure gradient with an average pressure around -50Pa. Conversely, the pressure gradient captured by the URANS model is insignificant, which does not align with the actual situation. The LES model predicts a wider pressure distribution with a more even pressure and an average of around -60 Pa, while the pressure gradient is less. The DES model predicts a relatively wide pressure distribution, similar to that of the LES model, with an average pressure of around -40 Pa. These results suggest that the IDDES model is more appropriate for capturing the bus body pressure, and the LES model need not be considered in cost calculation. The URANS model captures insignificant pressure gradient changes and is not suitable for capturing bus body pressure.

Figure 11 depicts the vortices around the bus body, where the Q criterion (Dong et al., 2016) is used as the iso-surface to identify the size of the vortex with Q=1000. Q is defined as $0.5*[||\Omega||^2_F-||S||^2_F]$, where Ω and S are the vorticity tensor and the strain rate tensor, respectively. This criterion is a commonly used method for extracting and identifying vortices. It can be observed that LES model captures the most vortices due to its ability to accurately solve the motion of all turbulence scales above a certain scale through filtering processing, but the vortex at the rear of the bus is fewer than those captured by DDES, DES, and LES models. URANS model is not suitable for capturing the vortex. Trailing edge vortices exhibit small-scale structures and rapid spatial variations. URANS models typically have limited spatial resolution due to turbulence closure models and computational constraints. This limited resolution may result in inadequate capture of the intricate details of trailing edge vortices. At a distance from the bus, LES, IDDES and DES models catches many large vortice. To conduct a quantitative analysis of the pressure at the rear of the bus, six probes were established as shown in Fig. 12. Probes 1, 2, and 3 have the same y- and z-coordinates, while their x-coordinates correspond to 6, 5, and 4 m, respectively. Probes 4, 5, and 6 have the same x- and y-coordinates, while their z-coordinates correspond to 2.5, 1.5, and 0.5 m, respectively. Each probe has a resolution of 100 points to monitor the pressure. The pressure fluctuations of LES, IDDES, and DDES models on probe 1 are larger than those of DES and URANS models. On probe 2, the pressure fluctuations of LES model are significantly larger than those simulated by the other four turbulence models. However, the pressure fluctuations of LES and DDES models are similar and greater than those of the other three turbulence models. This indicates that LES can capture the vertical pressure fluctuation whether it is near or far from the rear of the bus. DDES can also capture the vertical pressure fluctuation far from the rear of the bus. At probes 5 and 6, the pressure fluctuation of IDDES model is greater than that of the other four turbulence models, suggesting that IDDES model has a stronger ability to capture the pressure fluctuation of the bus along the y-axis. In addition, URANS model has minimal fluctuation. At probe 4 and 5, DDES, DES and LES models are similar and have small fluctuations in capturing pressure.

3.3 Flow Field in the Middle of Bus Body

In Fig. 13, the pressure, velocity, and velocity streamline for the x=0 section in the middle of the bus body are depicted. The results demonstrate that the IDDES model exhibits the widest range for capturing pressure, as well as the most accurate pressure distribution around the bus body compared to the other turbulence models. This can be attributed to the fact that

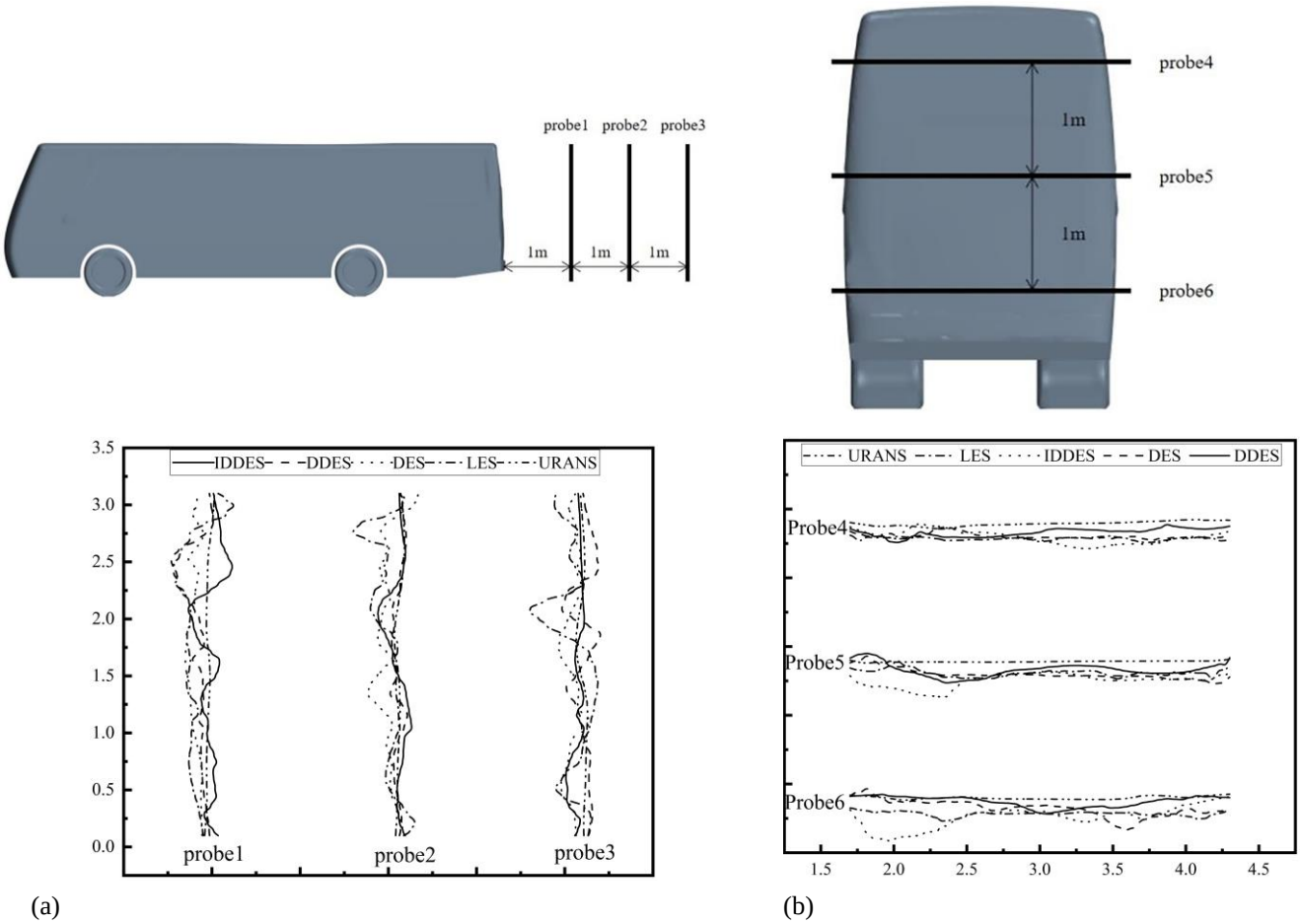

Fig 12 Velocity profiles in the wake behind the rear body. (a) vertical; (b) horizontal

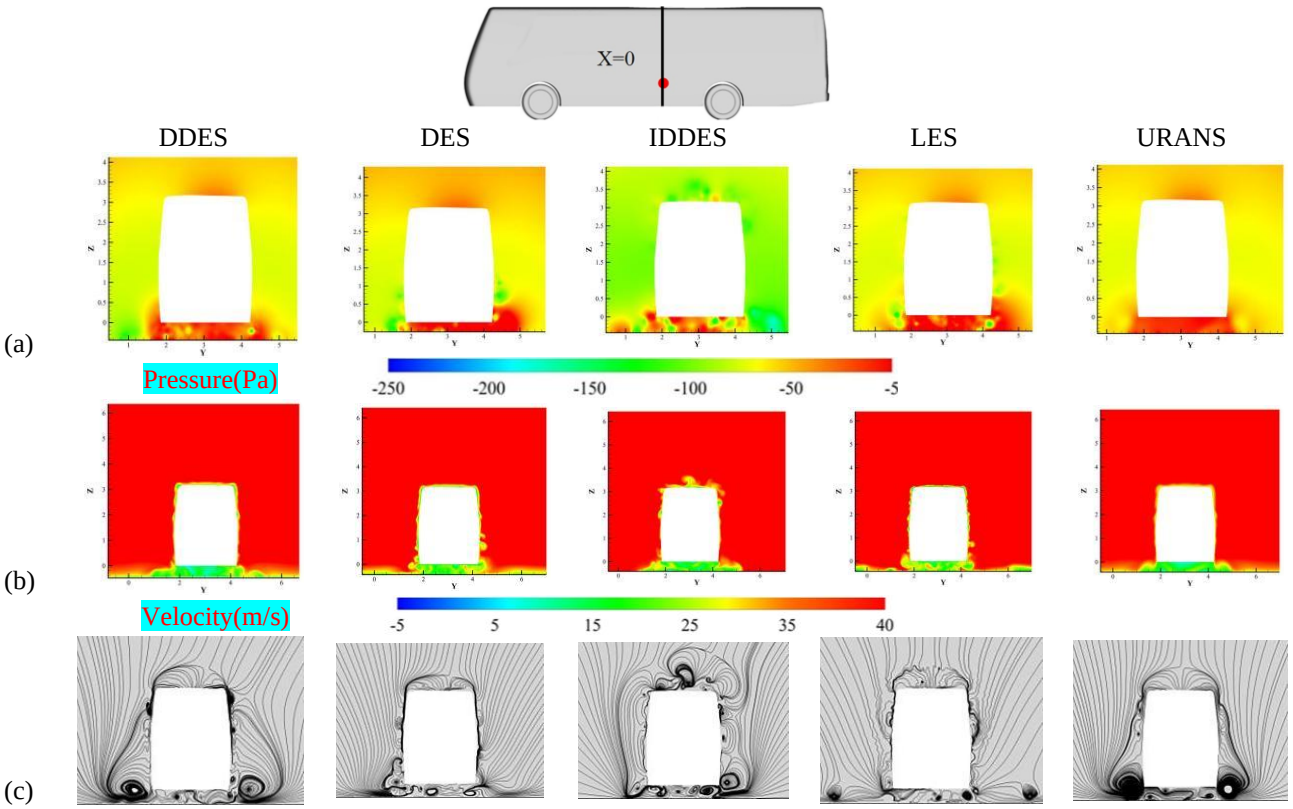

Fig. 13 Pressure, velocity, and streamline distributions on x=0: (a) pressure; (b) velocity; (c) streamline

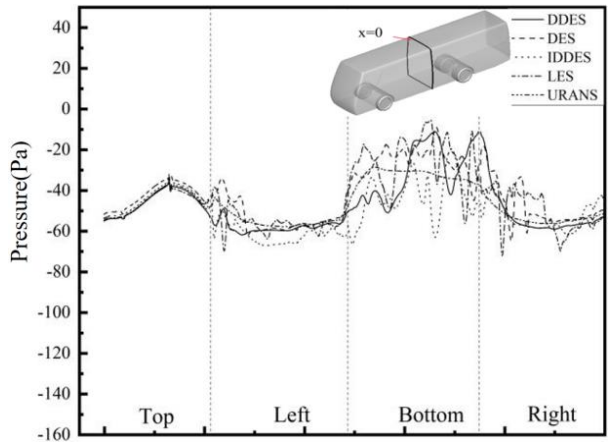

Fig. 14 Pressure distribution on x=0

the minimum negative pressure obtained by the IDDES model is lower than that of the other four models, leading to a greater pressure gradient. Conversely, the URANS model does not exhibit a small negative pressure, which can be explained by the complex turbulence at the bottom of the bus resulting in an uneven pressure distribution. This phenomenon is well-captured by the IDDES model.

Figure 13(b) displays the velocity field around the middle section of the bus body. A large vortex on the roof of the bus, which is captured by the IDDES model, suggests that it performs better in capturing turbulence at the top of the bus. The turbulence obtained by the DDES and IDDES models at the bottom is more complex compared to that of the LES and DES models. However, the URANS model captures few details of the turbulence.

Figure 13(c) depicts the streamline at the middle section of the bus body. The LES model is capable of capturing numerous fine vortices around the body, demonstrating its superior ability to capture the overall turbulence. However, the streamline captured by the URANS model exhibits unreasonable symmetry. The DDES model also displays symmetry in capturing vortices around the body, but numerous vortices are observed near the bus body. This finding implies that the DDES model is stronger in capturing vortices near the wall than those far from the wall. Notably, the IDDES model captures fine vortices on the top and around the bus body, indicating that it is more accurate in predicting air flow trajectory. The IDDES model combines the advantages of RANS and LES to achieve higher spatial resolution in the near-wall and vortex formation regions. This higher resolution grid enables more accurate capture of small-scale vortex structures.

Figure 14 displays the pressure distribution at x=0. The results demonstrate that DDES, LES and DES models exhibit a larger average pressure difference between the bottom and top compared to URANS and IDDES models. Consequently, DDES, LES and DES models can generate greater lift than IDDES and URANS models, which could compromise the adhesion of the bus and compromise driving safety. On the other hand, IDDES model exhibits the smallest average pressure difference between the top and bottom. Furthermore, IDDES model also has a smaller average pressure difference between the left and right than the other four turbulence models.

4. CONCLUSION

This study investigates the aerodynamic performance of a bus using five distinct turbulence models. The simulations were carried out using the grid refinement method, and the accuracy of the turbulence models was confirmed by comparing the numerical results with Wind tunnel test data. The velocity field, pressure field, and streamline of the bus were thoroughly analyzed and compared for the five turbulence models at both the rear and middle sections of the bus.

The drag coefficient obtained from the IDDES model is closest to the experimental results. The results show that the IDDES model accurately captures the larger negative pressure at the rear of the bus, as well as the pressure further away from the rear. Similar to the DDES model, IDDES can effectively resolve the pressure gradients at the rear of the bus. Furthermore, the IDDES model was found to capture turbulence at the top of the rear and had a wider range for wake flow at the rear. On the other hand, DDES exhibited clear shedding in the wake. The wake flow of LES was most even in the flow direction. The air flow trajectory of IDDES model was relatively smooth, as seen from the analysis of wake vortex and air flow trajectory. The LES, DES, DDES, and IDDES models are capable of forming a detailed and rich wake vortex at y=0. In contrast, the wake vortex formed by the URANS model at y=0 is relatively smooth and lacks some detailed descriptions. Notably, the IDDES model captured many small vortices around the bus body at x=0, while LES model captured fewer vortices.

This study provides important guidance for the selection of turbulence models in the research of bus aerodynamics and demonstrates the reliability of the IDDES model in studying bus aerodynamics. The results of this research are expected to have a positive impact on the study of bus aerodynamics. Future research can build upon the results of this study to further improve turbulence models and explore turbulence models that are more suitable for the study of bus aerodynamics. In addition, it is possible to compare the variations in velocity and pressure on the windward surface under different turbulence models.

ACKNOWLEDGEMENTS

This work was supported the National Key R&D program of China (2022YFB4003700). National Natural Science Foundation of China (Grant No. 52076072). Research Foundation of Education Bureau of Hunan Province (Grant No: 21A0396). Innovation and Entrepreneurship Training Program for College Students of Hunan Province (Grant No: S202212658008).

CONFLICT OF INTEREST

The authors declare that they have no known competing financial interests or personal relationships that could have appeared to influence the work reported in this paper.

AUTHORS CONTRIBUTION

Taiming Huang: Conceptualization, Methodology, Software, Data curation, Visualization, Writing – original draft, Supervision. **Jingmao Ma:** Software, Investigation. **Dingxun Yi:** Software, Investigation. **Xun Ren:** Software, Investigation. **Rongyi Ke:** Software, Investigation. **Changjie Ou:** Methodology, Software, Investigation, Writing – review & editing. **Qinglin Du:** Investigation. **Qiang Huang:** Investigation. **Wei Zeng:** Validation, Resources, Writing – review & editing.

REFERENCE

Alonso-Estébanez, A., Del Coz Díaz, J. J., Álvarez Rabanal, F. P. & Pascual-Muñoz, P. (2017). Numerical simulation of bus aerodynamics on several classes of bridge decks. *Engineering Applications of Computational Fluid Mechanics*, *11*(1), 435-449. https://doi.org/10.1080/19942060.2016.1201544

Altaf, A., Omar, A. A., & Asrar, W. (2014). Passive drag reduction of square back road vehicles. *Journal of Wind Engineering and Industrial Aerodynamics*, *134*, 30-43. https://doi.org/10.1016/j.jweia.2014.08.006

Anzalotta, C., Joshi, K., Fernandez, E., & Bhattacharya, S. (2020). Effect of forcing the tip-gap of a NACA0065 airfoil using plasma actuators: A proof-of-concept study. *Aerospace Science and Technology*, *107*, 106268. https://doi.org/10.1016/j.ast.2020.106268

Argyropoulos, C. D., & Markatos, N. C. (2015). Recent advances on the numerical modelling of turbulent flows. *Applied Mathematical Modelling*, *39*(2), 693-732. https://doi.org/10.1016/j.apm.2014.07.001

Ashagrie, G., Nallamothu, R. B., Nallamothu, A. K., & Nallamothu, S. K. (2017). A study on driving stability of bus using computational fluid dynamics (CFD). *International Journal for Research in Applied Science & Engineering Technology*, *5*(11). https://www.researchgate.net/publication/322234213

Bhattacharya, S., & Ahmed, A. (2010). *Effect of sinusoidal forcing on the wake of a circular cylinder*. 48th AIAA Aerospace Sciences Meeting Including the New Horizons Forum and Aerospace Exposition.

Chang, Y., Yang, Z., & Li, Q. (2021). Numerical and experimental research on flow and aerodynamic noise characteristics of coach. *Proceedings of the Institution of Mechanical Engineers, Part D: Journal of Automobile Engineering*, *235*(6), 1685-1701. https://doi.org/10.1177/0954407020973816

Chaouat, B. (2017). The state of the art of hybrid RANS/LES modeling for the simulation of turbulent flows. *Flow, Turbulence and Combustion*, *99*(2), 279-327. https://doi.org/10.1007/s10494-017-9828-8

Cheng, S. Y., Tsubokura, M., Nakashima, T., Nouzawa, T., & Okada, Y. (2011). A numerical analysis of transient flow past road vehicles subjected to pitching oscillation. *Journal of Wind Engineering & Industrial Aerodynamics*, *99*(5), 511-522. https://doi.org/10.1016/j.jweia.2011.02.001

Deck, S., & Renard, N. (2020). Towards an enhanced protection of attached boundary layers in hybrid RANS/LES methods. *Journal of Computational Physics*, *400*. https://doi.org/10.1016/j.jcp.2019.108970

Dong, Y., Yan, Y., & Liu, C. (2016). New visualization method for vortex structure in turbulence by lambda2 and vortex filaments. *Applied Mathematical Modelling*, *40*(1), 500-509. https://doi.org/10.1016/j.apm.2015.04.059

Dorigatti, F., Sterling, M., Rocchi, D., Belloli, M., Quinn, A. D., Baker, C. J., & Ozkan, E. (2012). Wind tunnel measurements of crosswind loads on high sided vehicles over long span bridges. *Journal of Wind Engineering and Industrial Aerodynamics*, *107*, 214-224. https://doi.org/10.1016/j.jweia.2012.04.017

Duraisamy, K., Iaccarino, G., & Xiao, H. (2019). Turbulence modeling in the age of data. *Annual Review of Fluid Mechanics*, *51*(1). https://doi.org/10.1146/annurev-fluid-010518-040547

François, D. G., Delnero, J. S., Colman, J., Marañón, D. L. J., & Camocardi, M. (2009, January). *Experimental determination of Stationary Aerodynamics loads on a double deck Bus*. 11th Americas Conference on Wind Engineering, San Juan, Puerto Rico. http://www.iawe.org/Proceedings/11ACWE/11ACWE-MaranonDiLeo.pdf

Friess, C., Manceau, R., & Gatski, T. B. (2015). Toward an equivalence criterion for hybrid RANS/LES methods. *Computers & Fluids*, *122*, 233-246. https://doi.org/10.1016/j.compfluid.2015.08.010

Garcia-Ribeiro, D., Bravo-Mosquera, P. D., Ayala-Zuluaga, J. A., Martinez-Castañeda, D. F., Valbuena-Aguilera, J. S., Cerón-Muñoz, H. D., & Vaca-Rios, J. J. (2023). Drag reduction of a commercial bus with add-on aerodynamic devices. *Proceedings of the Institution of Mechanical Engineers, Part D: Journal of Automobile Engineering*, *237*(7), 1623-1636. https://doi.org/10.1177/09544070221098209

Gilotte, P., Mortazavi, I., Colon de Carvajal, A., Edwige, S., & Nayeri, C. N. (2022). Aerodynamical characteristics of a reduced scale ground vehicle according to yaw angle variations. *International Journal of Numerical Methods for Heat & Fluid Flow*, *32*(4), 1222-1236. https://doi.org/10.1108/HFF-08-2021-0522

Gu, Z. Q., Huang, T. M., Chen, Z., Zong, Y. Q., & Zeng, W. (2016). Large eddy simulation of the flow-field around road vehicle subjected to pitching motion. *Journal of Applied Fluid Mechanics*, *9*(6), 2731-2741.

https://doi.org/10.29252/jafm.09.06.25330

He, K., Minelli, G., Wang, J., Gao, G., & Krajnovi, S. (2021). Assessment of les, iddes and rans approaches for prediction of wakes behind notchback road vehicles. *Journal of Wind Engineering and Industrial Aerodynamics*, *217*, 104737. https://doi.org/10.1016/j.jweia.2021.104737

He, K., Su, X., Gao, G., & Krajnovi, S. (2022). Evaluation of les, iddes and urans for prediction of flow around a streamlined high-speed train. *Journal of Wind Engineering and Industrial Aerodynamics*, *223*, 104952. https://doi.org/10.1016/j.jweia.2022.104952

Huang, T. M., Gu, Z. Q., & Feng, C. J. (2017). Coupled analysis of unsteady aerodynamics and vehicle motion of a passenger car in crosswind condition. *Journal of Applied Fluid Mechanics*, *10*(2), 625-637. https://doi.org/10.18869/acadpub.jafm.73.239.26639

Huang, T., Feng, M., Huang, J., Ma, J., Yi, D., Ren, X., & Ou, C. (2023). Aerodynamic stability of vehicle passing through a bridge tower at high speed under crosswind conditions with different road adhesion coefficients. *Alexandria Engineering Journal*, *77*, 461-478. https://doi.org/10.1016/j.aej.2023.07.001

Jadhav, C. R., & Chorage, R. P. (2020). Modification in commercial bus model to overcome aerodynamic drag effect by using CFD analysis. *Results in Engineering*, *6*, 100091. https://doi.org/10.1016/j.rineng.2019.100091

Joshi, K., & Bhattacharya, S. (2019). Large-eddy simulation of the effect of distributed plasma forcing on the wake of a circular cylinder. *Computers & Fluids*, *193*, 104295. https://doi:10.1016/j.compfluid.2019.104295

Joshi, K., Latrobe, B., & Bhattacharya, S. (2023). Altering the wake dynamics of a circular cylinder with harmonic forcing. *Physics of Fluids*, *35*(6). https://doi.org/10.1063/5.0153359

Kanekar, S., Thakre, P., & Rajkumar, E. (2017). *Aerodynamic study of state transport bus using computational fluid dynamics*. IOP Conference Series: Materials Science and Engineering. https://doi.org/10.1088/1757-899x/263/6/062052

Kongwat, S., Jongpradist, P., & Hasegawa, H. (2020). Lightweight bus body design and optimization for rollover crashworthiness. *International Journal of Automotive Technology*, *21*, 981-991. https://doi.org/10.1007/s12239-020-0093-9

Krajnovic, S., & Davidson, L. (2003). Numerical study of the flow around a bus-shaped body. *Journal of Fluids Engineering*, *125*(3), 500-509. https://doi.org/10.1115/1.1567305

Li, L., You, S., & Yang, C. (2016). Multi-objective stochastic MPC-based system control architecture for plug-in hybrid electric bus. *IEEE Transactions on Industrial Electronics*, *63*(8), 4752-4763. https://doi.org/10.1109/TIE.2016.2547359

Menter, F. R. (1994). Two-equation eddy-viscosity turbulence models for engineering applications. *AIAA Journal*, *32*(8), 1598-1605. https://doi.org/10.2514/3.12149

Mockett, C., Fuchs, M., Garbaruk, A., Shur, M., Spalart, P., Strelets, M., & Travin, A. (2015). Two non-zonal approaches to accelerate RANS to LES transition of free shear layers in DES. *Progress in Hybrid RANS-LES Modelling*, *130*, 187-201. https://doi.org/10.1007/978-3-319-15141-0-15

Mohamed, E. A., Radhwi, M. N., & Abdel Gawad, A. F. (2015). Computational investigation of aerodynamic characteristics and drag reduction of a bus model. *American Journal of Aerospace Engineering*, *2*(1-1), 64-73. https://doi.org/10.11648/j.ajae.s.20150201.16

Nived, M. R., Mukesh, B. S., Athkuri, S. S. C., & Eswaran, V. (2022). On the performance of RANS turbulence models in predicting static stall over airfoils at high Reynolds numbers. *International Journal of Numerical Methods for Heat & Fluid Flow*, *32*(4), 1299-1323. https://doi.org/10.1108/HFF-08-2021-0519

Patel, N., He, M., Hemida, H., & Quinn, A. (2019). Large-eddy simulation of the airflow around a truck. *Journal of Wind Engineering and Industrial Aerodynamics*, *195*, 104017. https://doi.org/10.1016/j.jweia.2019.104017

Probst, A., & Melber-Wilkending, S. (2022). Hybrid RANS/LES of a generic high-lift aircraft configuration near maximum lift. *International Journal of Numerical Methods for Heat & Fluid Flow*, *32*(4), 1204-1221. https://doi.org/10.1108/HFF-08-2021-0525

Reddy, K. R., Ryon, J. A., & Durbin, P. A. (2014). A DDES model with a Smagorinsky-type eddy viscosity formulation and log-layer mismatch correction. *International Journal of Heat and Fluid Flow*, *50*, 103-113. https://doi.org/10.1016/j.ijheatfluidflow.2014.06.002

Renard, N., & Deck, S. (2015). Improvements in zonal detached eddy simulation for wall modeled large eddy simulation. *AIAA Journal*, *53*(11), 3499-3504. https://doi.org/10.1007/s00162-011-0240-z

Salari, K., & Ortega, J. M. (2021). Aerodynamic integration produces a vehicle shape with a negative drag coefficient. *Proceedings of the National Academy of Sciences*, *118*(27), e2106406118. https://doi.org/10.1073/pnas.2106406118

Serre, E., Minguez, M., Pasquetti, R., Guilmineau, E., Deng, G. B., Kornhaas, M., & Rodi, W. (2013). On simulating the turbulent flow around the Ahmed body: A French–German collaborative evaluation of LES and DES. *Computers & Fluids*, *78*, 10-23. https://doi.org/10.1016/j.compfluid.2011.05.017

Shur, M. L., Spalart, P. R., Strelets, M. K., & Travin, A. K. (2008). A hybrid RANS-LES approach with delayed-DES and wall-modelled LES capabilities.

International Journal of Heat and Fluid Flow, *29*(6), 1638-1649. https://doi.org/10.1016/j.ijheatfluidflow.2008.07.001

Shur, M. L., Spalart, P. R., Strelets, M. K., & Travin, A. K. (2015). An enhanced version of DES with rapid transition from RANS to LES in separated flows. *Flow, Turbulence and Combustion*, *95*(4). https://doi.org/10.1007/s10494-015-9618-0

Spalart, P. R. (2009). Detached-eddy simulation. *Annual Review of Fluid Mechanics*, *41*(1), 181-202. https://doi.org/10.1146/annurev.fluid.010908.165130

Spalart, P. R. (2015). Philosophies and fallacies in turbulence modeling. *Progress in Aerospace Sciences*, *74*, 1-15. https://doi.org/10.1016/j.paerosci.2014.12.004

Tyliszczak, A., Cavaliere, D. E., & Mastorakos, E. (2014). LES/CMC of blow-off in a liquid fueled swirl burner. *Flow, Turbulence and Combustion*, *92*(1-2), 237-267. https://doi.org/10.1007/s10494-013-9477-5

Volpe, R., Devinant, P., & Kourta, A. (2015). Experimental characterization of the unsteady natural wake of the full-scale square back Ahmed body: flow bi-stability and spectral analysis. *Experiments in Fluids*, *56*(5), 1-22. https://doi.org/10.1007/s00348-015-1972-0

Wang, S., Bell, J. R., Burton, D., Herbst, A. H., Sheridan, J., & Thompson, M. C. (2017). The performance of different turbulence models (urans, sas and des) for predicting high-speed train slipstream. *Journal of Wind Engineering and Industrial Aerodynamics*, *165*, 46-57. https://doi.org/10.1016/j.jweia.2017.03.001

Winkler, N., Drugge, L., Trigell, A. S., & Efraimsson, G. (2016). Coupling aerodynamics to vehicle dynamics in transient crosswinds including a driver model. *Computers & Fluids*, *138*, 26-34. https://doi.org/10.1016/j.compfluid.2016.08.006

Yudianto, A., Adiyasa, I. W., & Yudantoko, A. (2021). Aerodynamics of bus platooning under crosswind. *Automotive Experiences*, *4*(3), 119-130. https://doi.org/10.31603/ae.5298

Yudianto, A., Sofyan, H., & Fauzi, N. A. (2022). Aerodynamic characteristics of overtaking bus under crosswind: CFD investigation. *CFD Letters*, *14*(8), 20-32. https://doi.org/10.37934/cfdl.14.8.2032

Zhang, Q., Su, C., & Wang, Y. (2020). Numerical investigation on aerodynamic performance and stability of a sedan under wind-bridge-tunnel road condition. *Alexandria Engineering Journal*, *59*(5), 3963-3980. https://doi.org/10.1016/j.aej.2020.07.004

Zhao, D., Zhang, D., & Chen, C. (2019, November). *Study on the Influence of Crosswind Angle and Longitudinal Spacing on bus in a Platoon*. IOP Conference Series: Materials Science and Engineering. https://doi.org/10.1088/1757-899X/688/2/022042

Zheng, L. D., Yang, Y., Qiang, G. L., & Gu, Z. (2022). Numerical analysis for wake flow field of Ahmed model based on a nonlinear-LRN/DES turbulence model. *International Journal of Numerical Methods for Heat & Fluid Flow*, *32*(4), 1348-1374. https://doi.org/10.1108/HFF-06-2021-0438